Coastline Extraction From SAR Data Using Doppler Centroid Images

Muhammad Amjad Iqbal, *Graduate Student Member, IEEE*, Andrei Anghel, *Senior Member, IEEE*, and Mihai Datcu, *Fellow, IEEE*

***Abstract*— Coastline extraction by exploiting optical images is challenging during adverse weather conditions. This letter proposes coastline extraction from synthetic aperture radar (SAR) data. Since collecting in-situ data is expensive and not always possible, the Doppler parameter is used to delineate coastlines when neither in-situ data nor cloud-free optical images are available. We propose a novel coastline extraction method based on classic coastal dynamic variation, such as Doppler centroid (f_{DC}), since the coastline is static and has zero Doppler with respect to the dynamic sea-state. The results of the Doppler-based novel technique allow us to investigate the impact of natural hazards on coastline degradation. We compare the proposed method to state-of-the-art (SOA) coastline extraction methods based on polarimetric correlations and the reference method from Sentinel-2. The results show that using scattering from dual and cross-polarization for coastline extraction is more reliable than using co-polarization. Based on empirical distributions and using the constant false alarm rate (CFAR) method, the relevant threshold has been adapted to distinguish land and sea in an unsupervised manner. We compare the results of polarimetric and Sentinel-2 with Doppler-based coastline extraction, which emphasizes the accuracy of the proposed f_{DC} method for extracting coastlines at full resolution.**

***Index Terms*— Coastline extraction, constant false alarm rate (CFAR), Doppler parameters, polarization, synthetic aperture radar (SAR).**

I. Introduction

A COASTLINE is the area where land meets the ocean. Coastal areas are of great importance as they are the most dynamic environments in the world [1]. For coastal zone safety, coastline extraction at various times is a fundamental task. Moreover, coastline applications, such as estimating shoreline circulation parameters, require information about the land-sea boundary [2], [3]. Recently, the detection of coastlines has been carried out by exploiting optical images from Sentinel-2, which perform very well when cloud coverage is minimal [4]. When the weather is cloudy, this technique is not viable since cloud removal itself is a challenging task [5].

Manuscript received 17 May 2022; revised 7 August 2022; accepted 29 September 2022. Date of publication 13 October 2022; date of current version 28 October 2022. This work was supported by Marie Skłodowska-Curie Actions Innovative Training Networks (MSCA-ITNs) through the Multimodal Environmental Exploration Systems–Novel Technologies (MENELAOS-NT) under Grant GA 860370. *(Corresponding author: Muhammad Amjad Iqbal.)*

Muhammad Amjad Iqbal and Andrei Anghel are with the CEO SpaceTech Research Center for Spatial Information, University Politehnica of Bucharest (UPB), 011061 Bucharest, Romania (e-mail: muhammad.iqbal@upb.ro; andrei.anghel2407@upb.ro).

Mihai Datcu is with the German Aerospace Center (DLR), 82234 Oberpfaffenhofen, Germany (e-mail: mihai.datcu@dlr.de).

Digital Object Identifier 10.1109/LGRS.2022.3214496

In practice, synthetic aperture radar (SAR) data has been used in a wide range of Earth Observation (EO) applications, such as the creation of digital elevation models, the detection of changes in the terrestrial surface, and the monitoring of displacements such as landslides, infrastructure, and coastline extraction. Due to the high resolution of SAR, its ability to overcome most weather constraints, and the impact of day and night time [6], [7], [8]. However, the dynamic nature of ocean waves, speckle noise from land, and coastal contrast make the coastline difficult to interpret. The interaction of radar electromagnetic waves with coastlines is significantly influenced by surface roughness and impacted by radar wavelength, incidence angle, and polarization. Numerous studies have shown that using SAR data from co-polarization VV/HH for coastline extraction mainly depends on radar incidence angle [9], [10]. Co-polarization with a lower incidence angle usually has inadequate contrast between land and sea. Coastline extraction is difficult and highly dependent on sea-state conditions, though it is feasible if the sea is calm.

In the literature, a method based on two-stage fuzzy processing and a trivial data combination is presented. This feature allows for the consideration of inaccuracy while reducing reliance on threshold and parameter values as much as possible [11]. This can be accomplished directly by empirical thresholding and simple image processing for the extraction of continuous coastlines. Furthermore, the linear feature of the coastline map can be detected by choosing a region of interest (ROI) from the SAR scene and by setting an empirical threshold for land and water separation [12], [13].

The stripmap (SM) single look complex (SLC) SAR is used for extraordinary events to provide high spatial resolution data with phase information. State-of-the-art (SOA) experiments conducted by researchers for the purpose of this study suggest that the majority of them used multipolarization and revealed that polarimetric-based extraction performed well. However, co-polarization correlation performance influenced when the incidence angle is $<30°$, whilst this polarization dependence is no longer applicable for incidence angles $>30°$ [10]. The polarimetric analysis of coastline extraction is performed in [6], [14], [15], [16], and [17] using the C and X bands SAR data. Given the correlation metrics, dual and cross polarizations have greater land/sea separation than co-polarization.

In this letter, we make use of SOA polarimetric combinations, including dual, cross, and co-polarization, to extract coastlines in a completely unsupervised approach. Therefore, from the smooth water region, an empirical distribution is

analyzed to apply a histogram-based threshold. Then, by using this threshold, logical images are generated that clearly differentiate the land and sea. The approach presented here works at full resolution with minimal loss caused by sliding window-based spatial mean operation. Moreover, it does not require any preprocessing or filtration. However, the output of the edge detector and information from geo-coded data are used to extract the coastline map.

The novel study involves determining the coastline based on the f_{DC}. Despite the fact that land is stationary and the ocean is dynamic, the significant difference in Doppler characteristics allows for straightforward extraction of coastline. In our scenario in-situ samples are unavailable for the study area. As a result, we use f_{DC} for coastline extraction and compare the results with Sentinel-2 and polarimetric coastline extraction. In addition, we analyze the footprint of Doppler parameters on coastline structure including velocity and height, which could be helpful for coastline engineering, monitoring, and management. High-resolution mapping of f_{DC}-based coastline extraction is covered by the scope of this letter.

II. Methodology

In this letter, we consider SM-SLC SAR datasets that contain partial polarimetric information, including co-polarized VV and cross-polarized scattering VH channels, respectively. Hence, the SAR data are S_{qq} and S_{pq}, where $p,\ q \in \{H, V\}$. A rough estimate is taken by evaluating the correlation coefficient to ensure that reflection symmetry is fulfilled and that both channels are uncorrelated [14]

$$\rho_c = \frac{\langle S_{qq} S_{pq}^{*} \rangle}{\sqrt{\langle |S_{qq}|^2 \rangle} \sqrt{\langle |S_{pq}|^2 \rangle}} \tag{1}$$

where $|\cdot|$, and $\langle \cdot \rangle$ represent modulus and spatial average correspondingly. The spatial averaging is carried out by using a sliding window of size 9×9, this size is selected to provide reliable estimates [14]. It is worth noting that ρ_c values are minimal over both land and sea, as we can observe in Fig. 1(c), demonstrating that reflection symmetry exists everywhere, moreover relative phase is unknown.

A. Coastline Extraction Based on Doppler Centroid

The novel case study focuses on coastline detection by extracting the Doppler variations around the coastline. On that account, the f_{DC} is the essence of this topic. Since incidence angle is $<30°$, therefore, we exploit the cross-polarized channel S_{pq}, to obtain better estimates of f_{DC}. Subsequently, as given in Fig. 2, to estimate f_{DC} we make use of correlation Doppler estimation (CDE) method which involves an auto-correlation of the SLC image with its shifted version in the azimuth direction "$\Delta\eta$" [18]. By using the sliding window "w" of size 9×9 we locally compute the correlation in the azimuth direction and perform an averaging operation in the range direction, ($\langle \cdot \rangle$, known as ensemble average). The phrase "ϕ" of correlation term $C(\eta, \tau)$ is estimated as

$$\phi(\eta, \tau) = \arg\left(\sum_{k=1}^{N} C(\eta, \tau_k) \right) \tag{2}$$

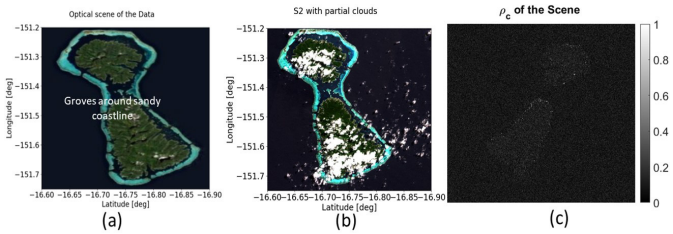

Fig. 1. (a) Optical image of the coastal site with grooves. (b) Sentinel-2 optical image with a dark time scan that is partially cloudy. (c) ρ_c describes the reflection symmetry that applies to both land and sea with minimal values.

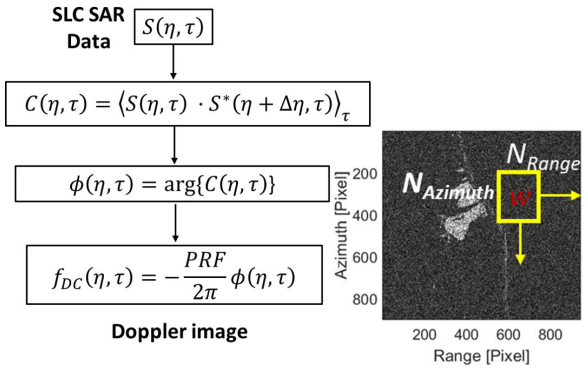

Fig. 2. CDE method to obtain f_{DC} image of SAR data by using a sliding window/box-car filter (w) of size $N \times N$.

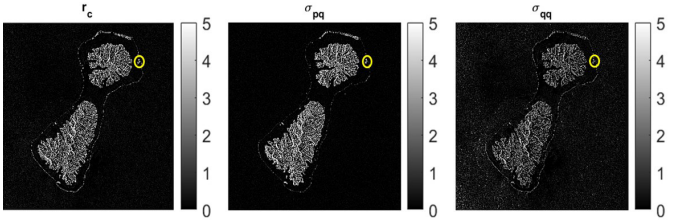

Fig. 3. Excerpt of SAR collected from an incidence angle of 26.5° over latitude −16.60 °N:−16.91 °S, and longitude −151.20 °W:−151.73 °E, on July 16, 2020, at 15 h:44 m:54 s. However, r_c, σ_{pq}, and σ_{qq} are evaluated and normalized over the same scale, whereas the yellow circle corresponds to ROI.

where N is the average number of cross correlation coefficients. Based on the pulse repetition frequency (PRF) and phase correlation function, the f_{DC} is calculated as follows:

$$f_{\mathrm{DC}}(\eta, \tau) = -\frac{\mathrm{PRF}}{2\pi}\phi(\eta, \tau). \tag{3}$$

The overall impression is that the coastline is static with respect to the sea and paves zero Doppler rate theoretically. Thus, dynamic and static natures easily distinguish the water and land. The next step is to extract the coastline while enhancing the land and water separation. Estimated f_{DC} is set to its absolute values for the sake of simplicity to use a single threshold value $|f_{\mathrm{DC}}^{[VH]}| = |f_{\mathrm{DC}}(\eta, \tau)|$. The constant false alarm rate (CFAR) method is applied over ROI which intends to provide a hetero-logical image from $f_{\mathrm{DC}}^{[VH]}$ at 2σ to clearly discriminate between land and sea. The CFAR method is discussed in Section II-B to obtain threshold "th."

B. Polarimetric Correlations for Coastline Extraction

The qualitative analysis associated with this research approach consists of both advancing the SOA in the

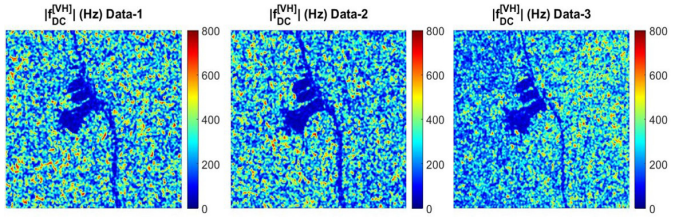

Fig. 4. $|f_{DC}|$ evaluated from [VH] polarization at ROI for three data sets, with a certain variation in Doppler rate. The separation between land and water is visible in the dynamic nature of sea-states. Datasets 1–3 are collected on July 10, 2019, July 16, 2020, and July 11, 2021, respectively.

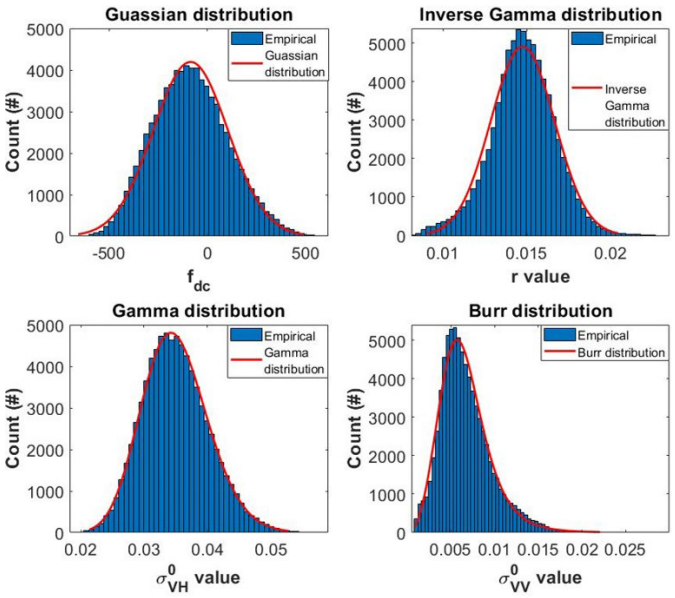

Fig. 5. Histograms evaluated within the smooth water region from ROI extracted from f_{DC}, r_c, σ_{pq}, and σ_{qq}, respectively, to observe the relevant distribution and find a threshold based on CFAR method to discriminate land and water. In a given data set, f_{DC}, r_c, σ_{pq}, and σ_{qq} closely follow Gaussian, inverse Gamma, Gamma, and Burr distributions, respectively.

delineation of coastlines with different polarizations and utilizing the f_{DC} to extract coastline maps. As a result, in Section II of this letter, coastline extraction is carried out using the metrics provided by [15], [16], and [17], which include correlation between co- and cross-polarized amplitude channels, as well as auto-correlations, given below

$$r_c = \langle |S_{pq}| \cdot |S_{qq}| \rangle, \quad \sigma_{pq} = \langle |S_{pq}|^2 \rangle, \quad \sigma_{qq} = \langle |S_{qq}|^2 \rangle. \quad (4)$$

The next step is to generate logical images to better visualize the land and water region separated. The histograms are evaluated to analyze the empirical distribution that is well approximated for each polarimetric combination and then adapt the relevant threshold, which is then applied to $|f_{DC}^{VH}|$, r_c, σ_{pq}, and σ_{qq}, images that provide logical binary and hetero-logical outputs in a robust manner. Upon that, [12], [15], and [20], provided the relationship between the probability of false alarm and CFAR threshold for Inverse Gamma, Gamma, Burr, and Gaussian distributions. Once the "th" values are obtained over smooth water region, the logical binary and hetero-logical outputs are obtained to distinguish sea and land easily. "th" values of $|f_{DC}^{VH}|$, r_c, σ_{pq}, and σ_{qq} over the ROI are varying for each distributions.

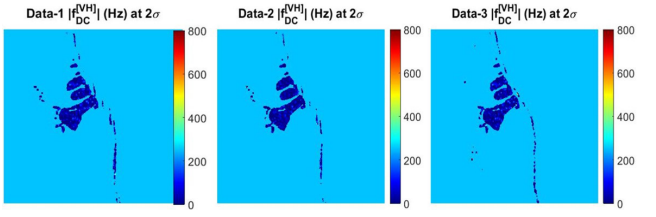

Fig. 6. Hetero-logical images of $|f_{DC}|$ at 2σ discriminating coastline and water for three data sets. The zero Doppler corresponds to land, while keeping sea-state homogeneous at 2σ.

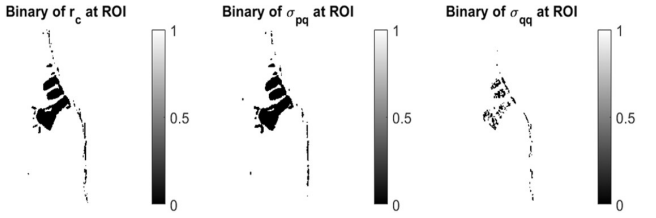

Fig. 7. Binary images obtained to discriminate land and water bodies over the ROI by using the threshold based on CFAR method, where r_c, σ_{pq}, and σ_{qq} follow inverse Gamma, Gamma, and Burr distribution, respectively.

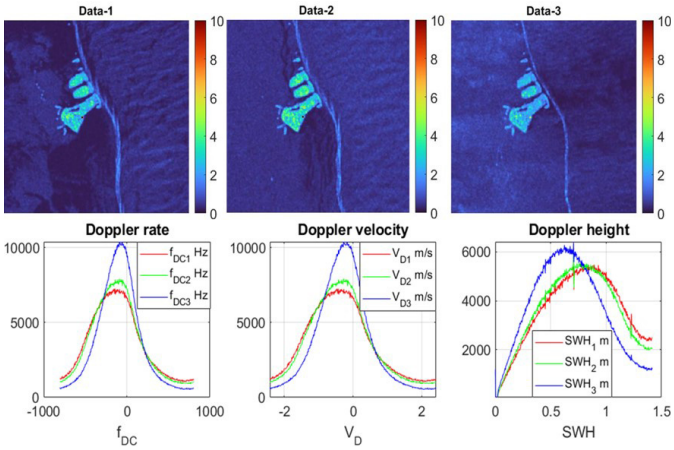

Fig. 8. Ocean circulation parameters are evaluated for three datasets in order to visualize the impact of each Doppler parameter on coastline structure.

III. Experimental Results

Experiments are carried out with SLC SM SAR data from Sentinel-1 from a coastal location with unique characteristics. The study region is centered around over latitude −16.60°N: −16.91°S, and longitude −151.20°W: −151.73°E, surrounded by the ocean and a thin, flat, and sandy coastline. The outside sandy shoreline incorporates grooves that allow ocean water to flow in and out of the island. Fig. 1(a) shows the optical image of the scene, and Fig. 1(b) represents the RGB image of Sentinel-2, influenced by partial clouds, however, ROI is cloud-free. The scene is challenging due to a very narrow and steep coastline. In Fig. 3, the given polarimetric correlation parameters r_c, σ_{pq}, and σ_{qq} are estimated from the scattering channels S_{pq} and S_{qq}. The values are normalized to mean values and the same scale is adopted to qualitatively show that the land and sea are well presented, while the sea area is homogeneous. However, for σ_{qq} sea state shows high back-scatterings which is an impact of a lower incidence angle ($26.5° < 30°$). In [4], [14], [15], [16], and [17], the extracted coastlines are mapped and overlapped with GPS

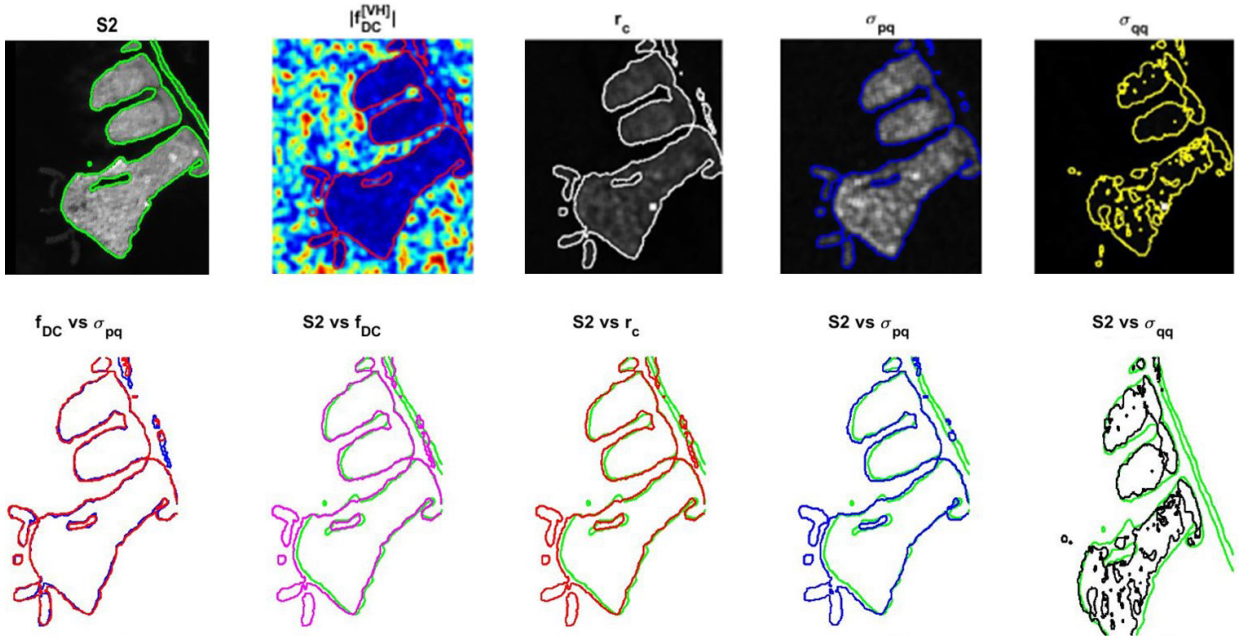

Fig. 9. Row one represents extracted coastline maps of Sentinel-2 (S2), $|f_{\mathrm{DC}}^{VH}|$, r_c, σ_{pq}, and σ_{qq} with their respective imagery over ROI related to the scene collected. Coastline map of S2 (green) is overlapped with $|f_{\mathrm{DC}}^{VH}|$ (magnetic), r_c (red), σ_{pq} (blue), and σ_{qq} (black) as shown row-2.

samples or Sentinel-2 data for quantitative analysis. For the given scene under observation, in-situ data are unavailable and Sentinel-2 data is partially cloudy, however, ROI is not affected by clouds. For the novel case, the f_{DC} is estimated to delineate the coastline and study dynamic variations. Due to the difference in the dynamic and static natures of the ocean and land/coastline, we use $|f_{\mathrm{DC}}|$ to extract the coastline and highlight its impact on the coastline.

The $|f_{\mathrm{DC}}|$ shown in Fig. 4 is influenced by dynamic Bragg waves and medium-scale variations. Fig. 5 shows the distribution of baseband f_{DC} for VH polarization for the given data set mentioned in Fig. 3, where we observe an empirical distribution over the smooth water from ROI, and utilize Gaussian distribution to obtain "th." However, due to the different f_{DC} and sea-state conditions value of "th" may vary from data to data. There exist false alarms after applying "th" because some pixels on the ocean area have zero Doppler, so to discard these false alarms we involve the former approach σ_{pq} to filter out. This criterion was chosen to isolate the variation caused by the sea dynamics and effectively extract the coastline. Fig. 6 depicts heterological images obtained from $|f_{\mathrm{DC}}|$ for three datasets in which the Doppler on the ocean surface is kept uniform at their 2σ values, to clearly distinguish the coastline from the sea surface. Data-1 and data-2 are showing very few false edges due to relatively high $|f_{\mathrm{DC}}|$ fluctuation, and observe a continuous coastline boundary in data-3. This analysis confirms the performance of the Doppler-based coastline extraction and allows us to adapt when in-situ data are unavailable. After obtaining logical images that clearly indicate land and sea, simple image processing and edge detection are used to retrieve the contour of coastline map.

To acquire the performance of SOA methods r_c, σ_{pq}, and σ_{qq}, in Fig. 5, the empirical histograms are evaluated over ROI, to highlight the ability of each selected distribution and "th" to discriminate between land and sea. Since polarization and their combinations differ, the distribution and "th" value varies from case to case, however, count density over the ROI remains constant in all scenarios. Empirical histograms quantitatively validate the theoretical distributions. To visually discriminate the land and sea, the next step is to generate the logical binary images from r_c, σ_{pq}, and σ_{qq} by using calculated values of threshold "th." In Fig. 7, the binary outputs show land and sea separation in an unsupervised way without any false edges, where logical *"1"* presents sea, while *"0"* corresponds to the land/coastline. The "Sobel" edge detector evaluates the binary and heterological image's 2-D spatial gradient and generates edges of the coastline. Overall, it appears that the detected line follows the coastline appropriately; no erroneous detection is seen. However, due to the relatively thin structure of the coastline boundary, there may be some missing pixels.

The detected coastline maps based on the above experiments are given in Fig. 9. We can observe maps of coastline obtained from $|f_{\mathrm{DC}}^{VH}|$, r_c, and σ_{pq}, having minimal variation with similar maps, besides σ_{qq} maps are erroneous due to the impact of lower incidence angle. The extracted coastline maps of the proposed $|f_{\mathrm{DC}}^{VH}|$ and σ_{pq} one of the SOA method in red and blue colors, respectively, are overlapped to quantify the accuracy of two methods, and a good agreement can be observed. Sentinel-2 (S2) image accurately detects the coastline and small water target, coastline map is highlighted with the green color given in Fig. 9 row one. The dataset of S2 was obtained in August 8, 2020. To quantify the performance, the overall agreement (OA) [4] is computed between S2 and both the proposed and SOA methods. The total number of pixel classified as sea, land, and both sea + land.

The quantitative analysis is reported in Table I by comparing the proposed and SOA methodologies with S2. We make

TABLE I
QUANTITATIVE ANALYSIS BASED ON OA

Comparison / OA	S2 vs $\lvert f_{DC}^{VH}\rvert$	S2 vs r_c	S2 vs σ_{pq}	S2 vs σ_{qq}
Land	0.3414	0.3418	0.3447	0.2524
Water	0.5799	0.5792	0.5693	0.6294
Land + Water	**0.9214**	0.9210	0.9140	0.8818

use of a good balance between the two classes, sea and land, the comparisons are carried out in a boundary chosen across the ROI. Experimental values of pixel classification for land and sea both together, show that $|f_{\mathrm{DC}}^{VH}|$ performs robust as r_c, σ_{pq}, however, σ_{pq} is under influence of incidence angle. Many industrial zones are located in coastal areas that might be at high risk of being affected by natural hazards like floods, tides, or currents. We describe the impact of such risks on the structure of coastline. The ocean circulation parameters are discussed in Fig. 8. The datasets are collected at various intervals in order to accurately predict the impact of Doppler parameters on coastline. We can observe that coastlines have variations in physical structures. The coastlines from data-1 and data-2 show that coasts are facing cuts and the sea state is slightly rough, which is an impact of high Doppler parameters. To study this footprint, we estimate Doppler velocity (V_D) [18], which varies up to 2.25 m/s and significant wave height (SWH) [19], which goes up to 1.45 m. The distributions of Doppler parameters of three data sets are presented in red, green, and blue plots, where data-3 (in blue) has the majority of its distribution around zero, which states the sea state condition is very calm. This study helps monitoring of coastline and delineates natural hazards to protect the shoreline. The proposed algorithm performs well in comparison with the SOA approach.

IV. CONCLUSION

In this letter, coastline extraction is done in an unsupervised way using the SM mode of SLC SAR data. A novel study of the Doppler centroid image-based coastline extraction is proposed. The $|f_{\mathrm{DC}}|$ estimated from the cross-polarized channel provides a better extraction of the coastline map. The proposed techniques process the entire scene very quickly using classical signal and image processing. The main features are the ability to work at full resolution and pixel-wise coastline detection. The quantitative analysis demonstrates that the accuracy of coastline extraction is satisfactory. The coastline map of $|f_{\mathrm{DC}}|$ is correctly extracted and compared to one of the SOA methods, σ_{pq}, and the reference Sentinel-2 image, where we find the highest OA when compared to other SOA methods. The analysis of Doppler's impact on the structure of the coastline allows us to monitor the shoreline under various circumstances and observe such anomalies. Future research will focus on optical images and the mapping of coastlines using GPS data. Time series from Sentinel-2 will also be integrated. These experiments pave the way for novel time-series analysis to infer coastline variations.

ACKNOWLEDGMENT

The authors appreciate the reviewer's insightful comments and technical suggestions, which significantly improved this letter.

REFERENCES

[1] J.-S. Lee and I. Jurkevich, "Coastline detection and tracing in SAr images," *IEEE Trans. Geosci. Remote Sens.*, vol. 28, no. 4, pp. 662–668, Jul. 1990.
[2] D. C. Mason and I. J. Davenport, "Accurate and efficient determination of the shoreline in ERS-1 SAR images," *IEEE Trans. Geosci. Remote Sens.*, vol. 34, no. 5, pp. 1243–1253, Sep. 1996.
[3] R. Gens, "Remote sensing of coastlines: Detection, extraction and monitoring," *Int. J. Remote Sens.*, vol. 31, no. 7, pp. 1819–1836, Apr. 2010.
[4] R. Pelich, M. Chini, R. Hostache, P. Matgen, and C. López-Martinez, "Coastline detection based on Sentinel-1 time series for ship- and flood-monitoring applications," *IEEE Geosci. Remote Sens. Lett.*, vol. 18, no. 10, pp. 1771–1775, Oct. 2021.
[5] O. Ghozatlou and M. Datcu, "Hybrid GAN and spectral angular distance for cloud removal," in *Proc. IEEE Int. Geosci. Remote Sens. Symp. (IGARSS)*, Jul. 2021, pp. 2695–2698.
[6] E. Ferrentino, A. Buono, F. Nunziata, A. Marino, and M. Migliaccio, "On the use of multipolarization satellite SAR data for coastline extraction in harsh coastal environments: The case of solway firth," *IEEE J. Sel. Topics Appl. Earth Observ. Remote Sens.*, vol. 14, pp. 249–257, 2021.
[7] A. Moreira, P. Prats-Iraola, M. Younis, G. Krieger, I. Hajnsek, and K. P. Papathanassiou, "A tutorial on synthetic aperture radar," *IEEE Geosci. Remote Sens. Mag.*, vol. 1, no. 1, pp. 6–43, Mar. 2013.
[8] M. Silveira and S. Heleno, "Separation between water and land in SAR images using region-based level sets," *IEEE Geosci. Remote Sens. Lett.*, vol. 6, no. 3, pp. 471–475, Jul. 2009.
[9] D.-J. Kim, W. M. Moon, S.-E. Park, J.-E. Kim, and H.-S. Lee, "Dependence of waterline mapping on radar frequency used for SAR images in intertidal areas," *IEEE Geosci. Remote Sens. Lett.*, vol. 4, no. 2, pp. 269–273, Apr. 2007.
[10] N. Baghdadi, R. Pedreros, N. Lenotre, T. Dewez, and M. Paganini, "Impact of polarization and incidence of the ASAR sensor on coastline mapping: Example of Gabon," *Int. J. Remote Sens.*, vol. 28, no. 17, pp. 3841–3849, Sep. 2007.
[11] S. Dellepiane, R. De Laurentiis, and F. Giordano, "Coastline extraction from SAR images and a method for the evaluation of the coastline precision," *Pattern Recognit. Lett.*, vol. 25, no. 13, pp. 1461–1470, Oct. 2004.
[12] E. Ferrentino, F. Nunziata, A. Buono, A. Urciuoli, and M. Migliaccio, "Multipolarization time series of Sentinel-1 SAR imagery to analyze variations of reservoirs' water body," *IEEE J. Sel. Topics Appl. Earth Observ. Remote Sens.*, vol. 13, pp. 840–846, 2020.
[13] J. Schou, H. Skriver, A. A. Nielsen, and K. Conradsen, "CFAR edge detector for polarimetric SAR images," *IEEE Trans. Geosci. Remote Sens.*, vol. 41, no. 1, pp. 20–32, Jan. 2003.
[14] F. Nunziata, A. Buono, M. Migliaccio, and G. Benassai, "Dual-polarimetric C- and X-band SAR data for coastline extraction," *IEEE J. Sel. Topics Appl. Earth Observ. Remote Sens.*, vol. 9, no. 11, pp. 4921–4928, Nov. 2016.
[15] F. Nunziata, M. Migliaccio, X. Li, and X. Ding, "Coastline extraction using dual-polarimetric COSMO-SkyMed PingPong mode SAR data," *IEEE Geosci. Remote Sens. Lett.*, vol. 11, no. 1, pp. 104–108, Jan. 2014.
[16] E. Ferrentino, F. Nunziata, and M. Migliaccio, "Full-polarimetric SAR measurements for coastline extraction and coastal area classification," *Int. J. Remote Sens.*, vol. 38, no. 23, pp. 7405–7421, 2017.
[17] X. Ding, F. Nunziata, X. Li, and M. Migliaccio, "Performance analysis and validation of waterline extraction approaches using single- and dualpolarimetric SAR data," *IEEE J. Sel. Topics Appl. Earth Observ. Remote Sens.*, vol. 8, no. 3, pp. 1019–1027, Mar. 2015.
[18] M. A. Iqbal, A. Anghel, and M. Datcu, "Doppler centroid estimation for ocean surface current retrieval from Sentinel-1 SAR data," in *Proc. 18th Eur. Radar Conf. (EuRAD)*, Apr. 2022, pp. 429–432.
[19] M. A. Iqbal, A. Anghel, and M. Datcu, "On the de-ramping of SLC-IW Tops SAR data and ocean circulation parameters estimation," in *Proc. IEEE Int. Geosci. Remote Sens. Symp. (IGARSS)*, Jul. 2022, pp. 6817–6820.
[20] C. Tison, J. M. Nicolas, F. Tupin, and H. Maitre, "A new statistical model for Markovian classification of urban areas in high-resolution SAR images," *IEEE Trans. Geosci. Remote Sens.*, vol. 42, no. 10, pp. 2046–2057, Oct. 2004.